Characteristics of Generalized Rectangular and Circular Ridge Waveguides

Yu Rong, *Senior Member, IEEE,* and Kawthar A. Zaki, *Fellow, IEEE*

***Abstract*—Generalized ridge waveguides are analyzed using the mode-matching method. The characteristic impedance, attenuation, and power-handling capability of several types of ridge rectangular waveguides and ridge circular waveguides are presented. Numerical results are obtained, which are useful in the design of many microwave components and subsystems.**

***Index Terms*—Attenuation, mode-matching method, power handling, ridged waveguide.**

I. Introduction

RIDGED waveguides have found many applications in microwave and millimeter-wave devices. Their advantages include large single-mode broad-band operation, large dominant cutoff wavelength, and low impedance characteristics. Early investigations were focused on properties of single- and double-ridge rectangular waveguides [1], [2]. Later, other structures were reported to be superior alternatives to the conventional single- and double-ridge waveguide. These structures include rectangular waveguides with one or two T-shaped septa [3], [4], two double-ridge waveguides [5], [6], antipodal ridge waveguides [7], double antipodal ridge waveguides [8], and quadruple-ridge waveguides [9]–[14]. Among these structures, the double antipodal ridge waveguide is of particular interest, because of its larger dominant mode cutoff wavelength, its proper use results in miniature compact components with superior electrical performance.

Attenuation and power-handling capabilities of the ridge waveguides are important parameters. For several types of ridge waveguides, these parameters cannot be found in the literature. To fill this gap and explore the potential applications of these waveguides, a general mode-matching approach is presented. This approach is applied to the analysis of different types of generalized ridge waveguides to get the attenuation and power-handling capabilities. Discussions are made and conclusions are drawn, which are very useful in practical applications.

II. Analysis Method

The general ridge waveguide configuration to be investigated is shown in Fig. 1. It is constructed by inserting an arbitrary number of rectangular ridges in the rectangular waveguide. For generality, the side planes M_1–M_1 and M_2–M_2 and the bottom planes A–A, B–B, $\cdots$, Q–Q could be either perfect electric wall (PEW) or perfect magnetic wall (PMW).

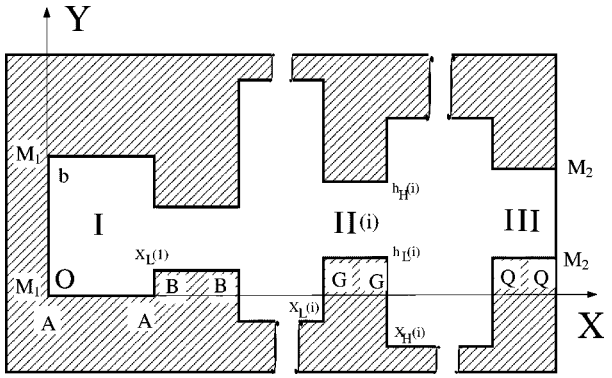

Fig. 1. The cross section of a general ridge waveguide.

To facilitate the analysis, this structure can be divided into three regions: Region I ($0 \le x \le X_L(1)$; $0 \le y \le b$), Region II ($\bigcup_{i=1}^{M}$ II(i), where II$(i) = (X_L(i) \le x \le X_H(i)$, $h_L(i) \le y \le h_H(i))$, $M = N - 1$ is the number of the subregions of Region II), and Region III ($X_L(N) \le x \le X_H(N)$, $h_L(N) \le y \le h_H(N)$). The modes of the ridge waveguides can be classified into TE and TM modes, and the transverse components can be obtained in terms of the longitudinal components H_z for TE mode, and E_z for TM mode [15]. TheE_z orH_z for TE and TM modes in each region m ($m =$ I, II$(i)(i = 1, 2, \cdots, M)$ and III) can be expressed as the superposition of eigenmodes as follows:

TE mode:

$$H^h_{z,m} = \sum_{n^h_m} h_{n^h_m}(x, y)e^{-\gamma_h z}. \tag{1}$$

TM mode:

$$E^e_{z,m} = \sum_{n^e_m} e_{n^e_m}(x, y)e^{-\gamma_e z} \tag{2}$$

where subscript m refers to the region m in Fig. 1, n^h_m and n^e_m are indexes of the modes taken in the region m for TE and TM mode, respectively, and γ_h and γ_e are propagation constants along the z-direction.$h_{n^h_m}(x, y)$ and $e_{n^e_m}(x, y)$ are eigenfunctions, which satisfy the following Helmholtz equation:

$$\left(\frac{\partial^2}{\partial x^2} + \frac{\partial^2}{\partial y^2}\right)\begin{Bmatrix} h_{n^h_m}(x, y) \\ e_{n^e_m}(x, y) \end{Bmatrix} + k^2_{c,q}\begin{Bmatrix} h_{n^h_m}(x, y) \\ e_{n^e_m}(x, y) \end{Bmatrix} = 0 \tag{3}$$

where $k_{c,q}$ ($q = e$ or h) refers to the cutoff wavenumber of the TE or TM mode, which satisfy $k^2_{c,q} + \gamma^2_q + \omega^2\mu\epsilon = 0$, ω

Manuscript received October 21, 1998.

Y. Rong was with the Department of Electrical and Computer Engineering, University of Maryland at College Park, College Park, MD 20742 USA. He is now with Paratek Microwave Inc., Columbia, MD 21045 USA.

K. A. Zaki is with the Department of Electrical and Computer Engineering, University of Maryland at College Park, College Park, MD 20742 USA.

Publisher Item Identifier S 0018-9480(00)00847-4.

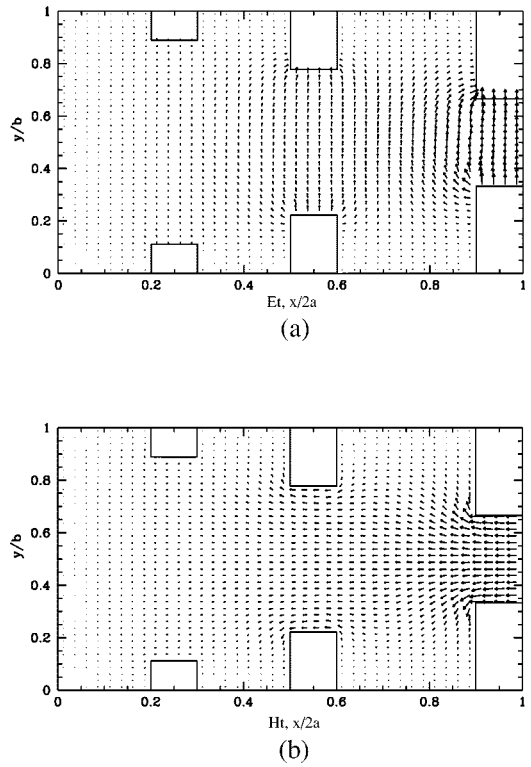

Fig. 2. (a) Electric fields in the waveguide. (b) Magnetic fields in the waveguide.

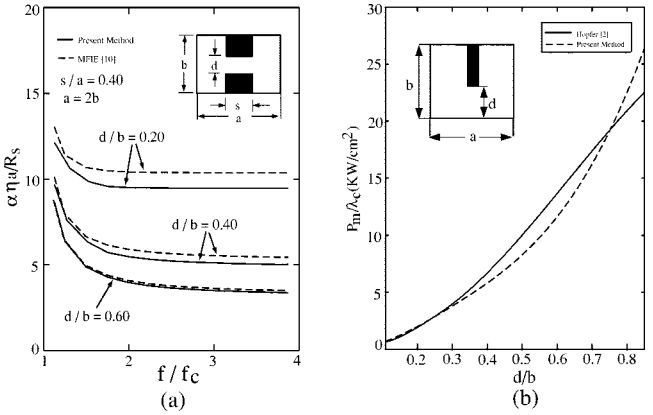

Fig. 3. (a) Attenuation comparison. (b) Power handling (without corner breakdown) comparison.

is the angular frequency, and μ and ϵ are the permeability and permittivity of the medium in the region. The general solution to the above equation can be written as follows:

$$\begin{Bmatrix} h_{n_m^h}(x,y) \\ e_{n_m^e}(x,y) \end{Bmatrix} = \left(A_m^q chk_{xm}^q x + B_m^q shk_{xm}^q x\right) \times \left(C_m^q \sin k_{ym}^q y + D_m^q \cos k_{ym}^q y\right) \quad (4)$$

where A_m^q, B_m^q, C_m^q, and D_m^q are field coefficients, which depend on the boundary conditions of region m. Either A_m^q or B_m^q and C_m^q or D_m^q could be eliminated by satisfying the boundary conditions along the x- and y-directions of the region m, respectively. k_{xm}^q and k_{ym}^q are the cutoff wavenumbers along the x- and y-directions, respectively, which satisfy $k_{xm}^{q2} - k_{ym}^{q2} + k_{c,q}^2 = 0$. k_{ym}^q equals $n_m^q \pi/[hh(m) - hl(m)]$

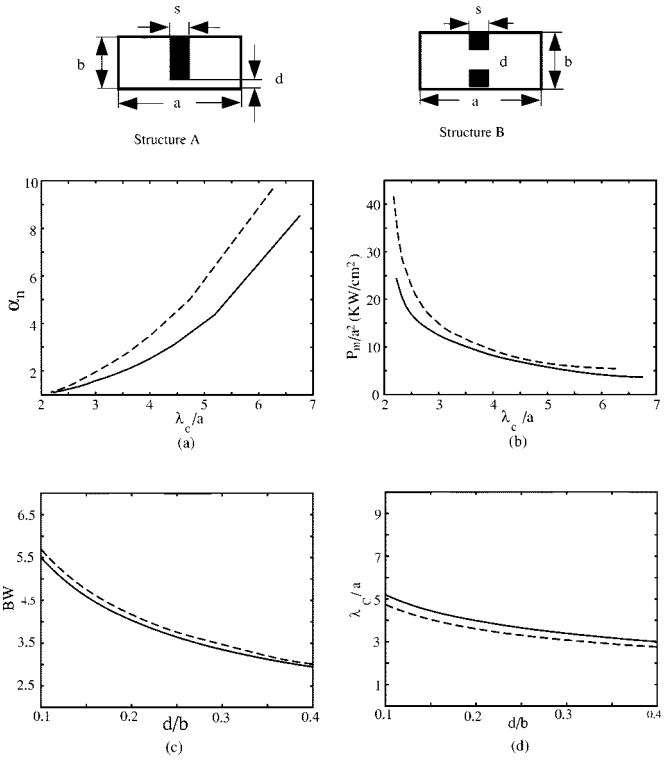

Fig. 4. (a) Attenuation, (b) power-handling, (c) bandwidth, and (d) dominant-mode cutoff λ_C versus d/b ($b/a = 0.45$, $s/a = 0.2$: Structure A, solid line; Structure B, dashed line).

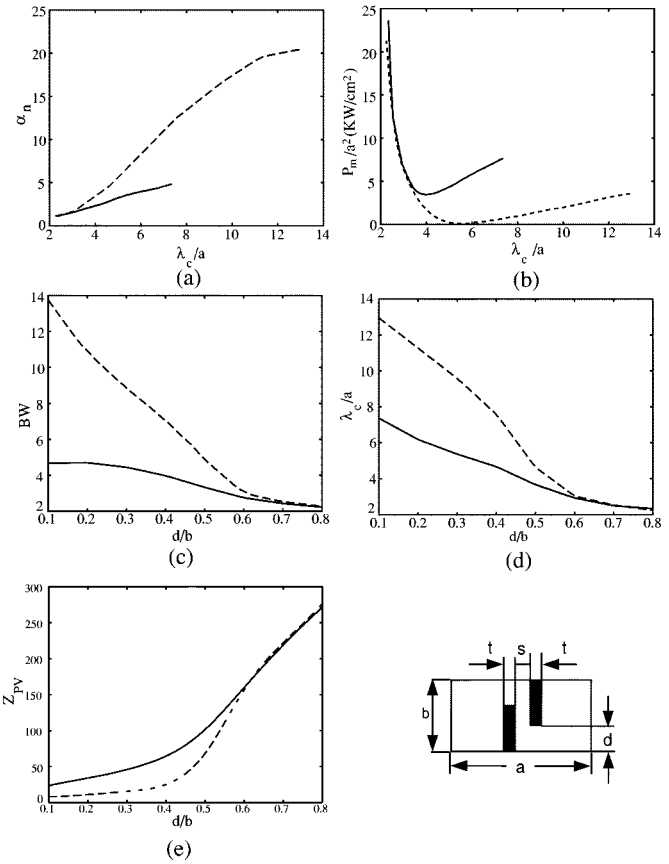

Fig. 5. (a) Attenuation, (b) power-handling, (c) bandwidth, and (d) dominant-mode cutoff λ_C versus d/b. (e) Characteristic impedance at $f = \infty$ ($b/a = 0.45$, $t/a = 0.1$: $s/a = 0.05$, solid line; $s/a = 0.01$, dashed line).

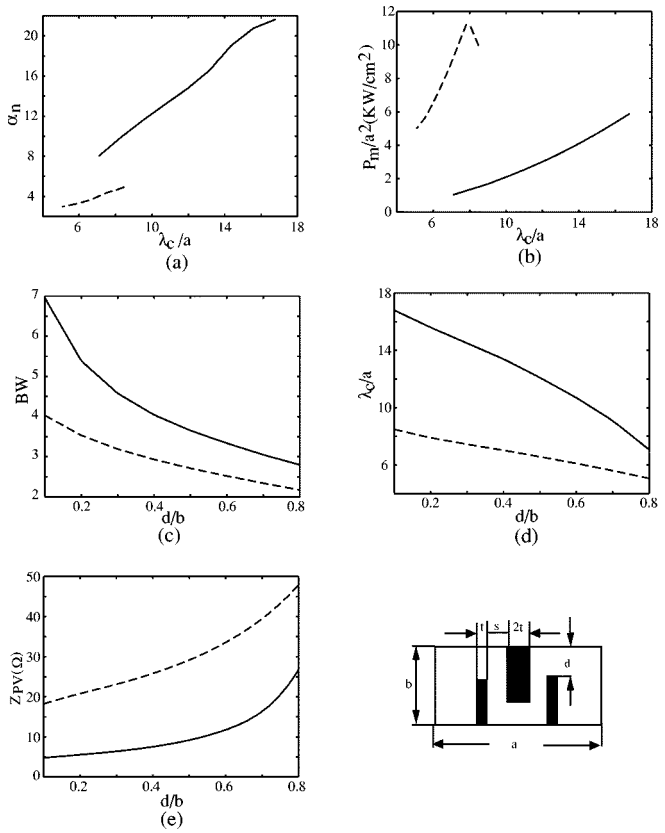

Fig. 6. (a) Attenuation, (b) power handling, (c) bandwidth, and (d) dominant-mode cutoff λ_C versus d/b. (e) Characteristic impedance at $f = \infty$ ($b/a = 0.45$, $t/a = 0.05$, $d_1/b = 0.15$: $s/a = 0.01$, solid line; $s/a = 0.05$, dashed line).

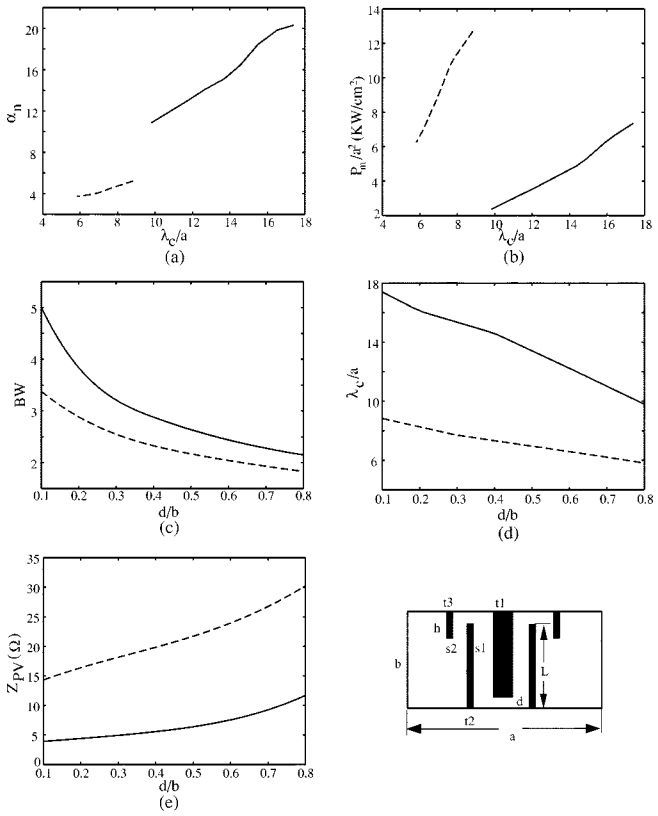

Fig. 7. (a) Attenuation, (b) power handling, (c) bandwidth, and (d) dominant-mode cutoff λ_C versus $s2/a$. (e) Characteristic impedance at $f = \infty$ ($b/a = 0.45$, $t_1/a = 0.2$, $t_2/a = t_3/a = 0.05$, $s_1 = s_2$, $L/b = 0.9$, $h/b = 0.2$: $s_1/a = 0.01$, solid line; $s_1/a = 0.05$, dashed line).

or $(2n_m^q + 1)\pi/2[hh(m) - hl(m)]$, depends on the property (PMW or PEW) of the bottom wall of the region m.

The boundary conditions on the interface (remaining boundary) between the arbitrarily adjacent regions i and $i+1 (i = 1, \cdots, N)$ are as follows:

$$\vec{E}_t|_i = \vec{E}_t|_{i+1}, \quad \vec{H}_t|_i = \vec{H}_t|_{i+1} + \vec{J}_t \tag{5}$$

where subscript t are the tangential components of the eigenfields and $\vec{J}_t$ is the tangential current on the interface. The unknown field coefficients in (4) can be found by matching the boundary conditions (5) at the interfaces between Regions I–III and by using the mode-matching method[16]. Using the orthogonality of the modes in the region and properly selecting the appropriate weighting functions to do the inner products for both sides of (5), a set of algebraic equations can be obtained, from which coefficient relations can be extracted.

A systematic and efficient method of successively matching the fields has been developed. Starting from the left-hand side of the generalized ridge waveguide, tangential fields at the boundary between Regions I and II(1) are matched first. Field coefficients in Region I can be expressed in terms of those in Region II(1). Fields at the boundary between Regions II(1) and II(2) are matched next. Field coefficients in Region II(1) are expressed in terms of those in Region II(2). This procedure can be repeated M times until all the fields at the boundaries in Region II are matched. Finally, the last boundary needed to be matched is the boundary between Regions II (M) and III. The final characteristic equation can be readily obtained. Truncating the numbers of modes in each subregion and setting the determinant of characteristic equation to zero leads to a set of algebraic equations. Solving this set of algebraic equations, the cutoff frequencies of TE and TM modes in the generalized ridge waveguide can be found. Substituting those obtained cutoff frequencies back into characteristic equation, the coefficients in Region III can be found. The field coefficients in Regions II and I are found by using the field coefficient relations found during the previous matching process. Therefore, fields in the whole region of the waveguide are found.

From field coefficients of the eigenmodes in the ridge waveguide, the attenuation and power handling can be calculated analytically. The attenuation constant α can be computed by using

$$\alpha = \frac{P_l}{2P_0} \tag{6}$$

where P_0 is the transmitted power in the waveguide and P_l is the surface conductor loss due to the surface current flowing at the ridge waveguide boundary, and can be obtained through the following equation:

$$P_l = \frac{R_s}{2} \oint |J_s^2|\, dl = \frac{R_s}{2} \oint |H_t^2|\, dl = \sum_{i=I}^{\text{III}} P_l^i \tag{7}$$

where the power loss is divided into several parts according to the metallic boundary of the ridge waveguide. Assuming that the electric field breaks down at the maximum field points when field intensity is E_b, the power-handling capacity of a general-

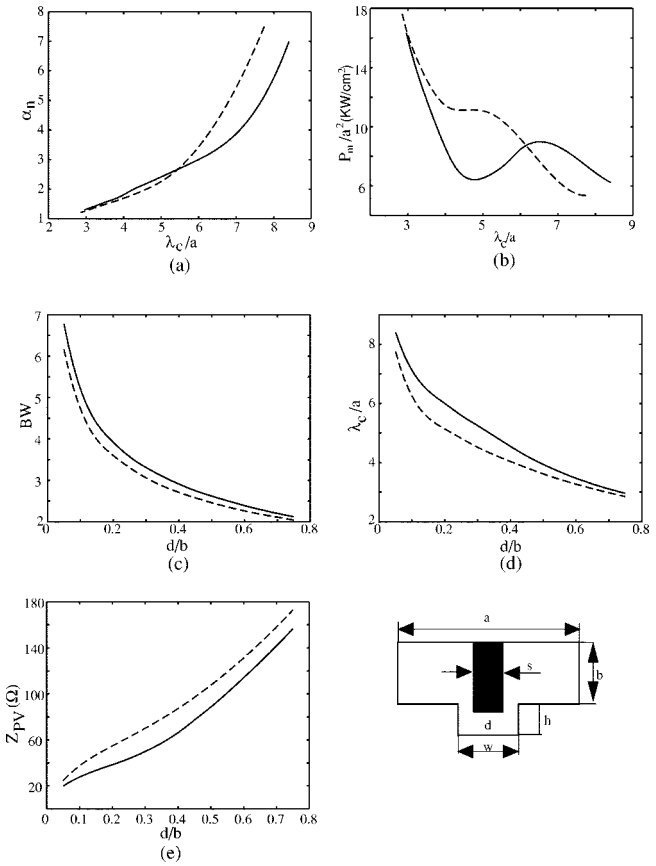

Fig. 8. (a) Attenuation, (b) power handling, (c) bandwidth, and (d) dominant-mode cutoff λ_C versus d/b. (e) Characteristic impedance at $f = \infty$ ($b/a = 0.45$, $h/b = 0.4$, $s/a = 0.2$: $w/a = 0.3$, solid line; $w/a = 0.4$, dashed line).

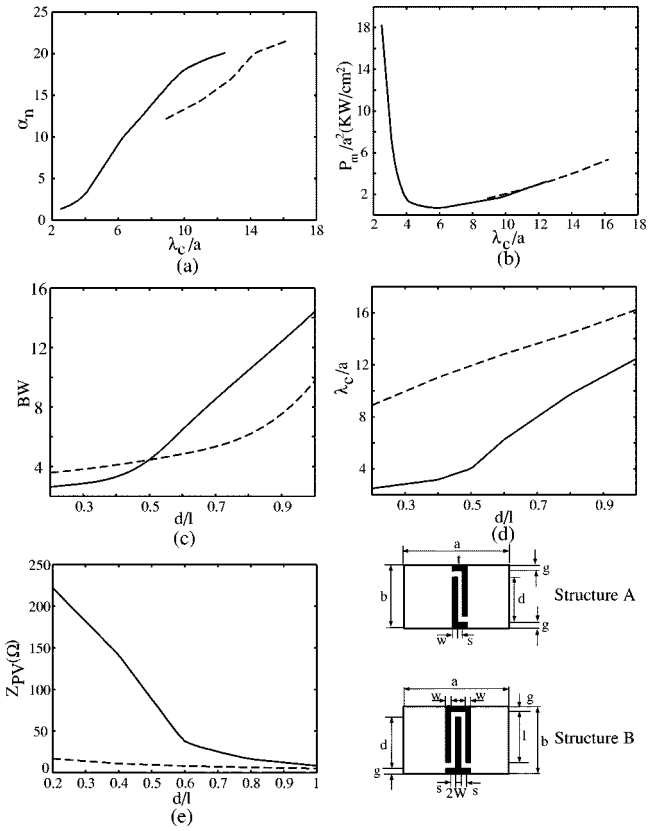

Fig. 9. (a) Attenuation, (b) power handling, (c) bandwidth, and (d) dominant-mode cutoff λ_C versus d/b. (e) Characteristic impedance at $f = \infty$ ($b/a = 0.45$, $s/a = 0.01$, $t/a = 0.2$, $g/b = 0.15$, $l/(b-2g) = 0.95$: Structure A ($t = 2w + s$), solid line; Structure B ($t = 4w + 2s$), dashed line).

ized ridge waveguide can be obtained by finding the maximum electric field in the waveguide. Suppose that the maximum electric field is $E_{\max}$, then the upper limit of the transmitted power $P_{\max}$ in the waveguide can be computed through the following:

$$P_{\max} = \frac{E_b^2}{E_{\max}^2} P_0. \tag{8}$$

The normalized attenuation α_n is defined as the ratio of the ridge waveguide attenuation to the zero-ridge waveguide attenuation, evaluated at the frequency $f = \sqrt{3} f_c$. The power handling is indicated by P_m, which represents the power carried by the waveguide at infinite frequency with the maximum electrical intensity $E_{\max}$ in the waveguide being equal to the breakdown field E_b. Generally, E_b can be expressed as 30/k (kv/cm), where k is factor ranging from 2 to 1 for short pulses to as much as 12 to 1 for continuous wave (CW) [17], [18]. Since E_b is assumed to be 30 kv/cm in the numerical calculation, the actual maximum normalized propagating power at any frequency is obtained by multiplying P_m by $\sqrt{1-(f_c/f)^2}/k^2$, in which k is determined by different applications.

To compare the properties of different ridge waveguides, relative bandwidth [2] is used. This relative bandwidth is defined as the ratio of λ_{c1} to λ_{c2}, where λ_{c1} corresponds to the cutoff wavelength of the dominant mode and λ_{c2} corresponds to the cutoff wavelength of the first higher order mode. To explore the applications of the different ridge waveguides, characteristic impedances $Z_{pv}|_{f=\infty}$, which is defined as follows, are also provided:

$$Z_{pv}|_{f=\infty} = V^2/P_0|_{f=\infty} \tag{9}$$

where V is gap voltage, which equals $\int_l \vec{E} \cdot \vec{dl}$. For the symmetric ridge waveguides, this integral is evaluated across the ridge gap along the symmetric plane. For the asymmetric ridge waveguides, this integral is evaluated across the ridge gap along the line which is the nearest to the middle plane. Characteristic impedances at any frequency is given by dividing $Z_{pv}|_{f=\infty}$ by the factor $\sqrt{1-(f_c/f)^2}$.

III. Numerical Results and Discussions

To validate the formulation and verify the accuracy of this approach, several checks of the numerical results are made. First, the vector fields in the waveguide are calculated and plotted, as shown in Fig. 2. It is clear that all the boundary conditions are satisfied. Second, the numerical results are compared with the analytical results when all the ridges are reduced to zeros. The normalized attenuationα_n becomes one and power handling is in agreement with that in [19]. Third, we compare the numerical results with those published in the literature, as shown in Fig. 3. Good agreement is obtained and, therefore, accuracy of the approach is established.

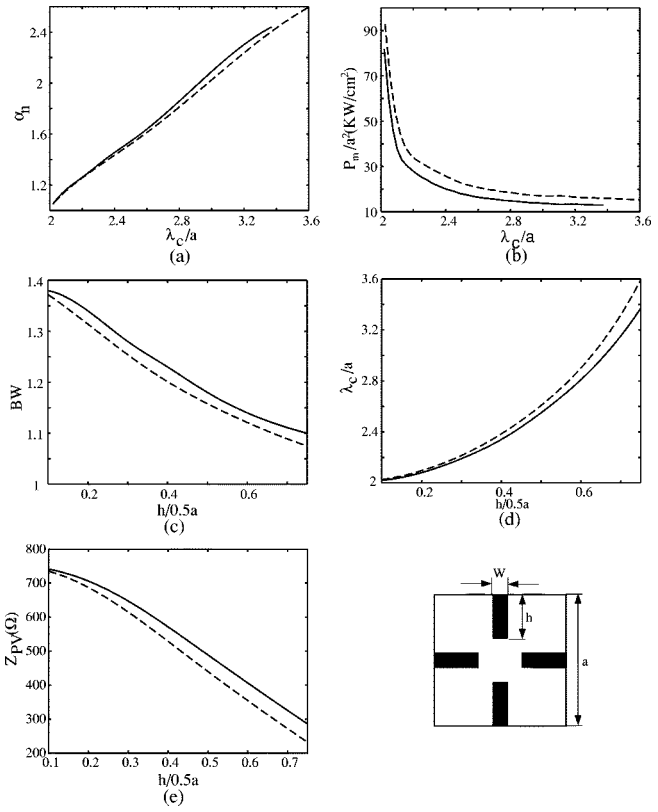

Fig. 10. (a) Attenuation, (b) power handling, (c) bandwidth, and (d) dominant-mode cutoff λ_C versus d/b. (e) Characteristic impedance at $f = \infty$ ($w/a = 0.05$, solid line; $w/a = 0.1$: dashed line).

The attenuation and power-handling capability in several ridge waveguides are presented. For reference, Fig. 4 shows the attenuation, power handling, dominant-mode cutoff wavelength, and relative bandwidth in the single- and double-ridge rectangular waveguide.

A. Ridged Rectangular Waveguide

1) Antipodal Ridge Rectangular Waveguides: The attenuation and power-handling capabilities in the antipodal ridge rectangular waveguides and double antipodal ridge rectangular waveguides are shown in Fig. 5 and 6. From these figures, it can be concluded that antipodal ridge rectangular waveguides and double antipodal ridge rectangular waveguides have almost the same characteristics. Compared to single ridge rectangular waveguides, the attenuation and power handling in both of these structures are improved. The dominant-mode cutoff wavelengths are much longer than those in single-ridge rectangular waveguides, which mean more compact components with low loss and higher power handling capabilities can be fabricated. With more antipodal ridges in the rectangular waveguides, as shown in Fig. 7, the dominant-mode wavelengths increase and power-handling capabilities improve. However, the bandwidth becomes narrower.

2) Ridge–Trough Rectangular Waveguides: Fig. 8 shows the attenuation and power-handling capabilities in ridge–trough rectangular waveguides, which are used in design of microwave wafer probe [20]. The bandwidth of the ridge–trough rectangular waveguide is narrower than the single-ridge rectangular waveguide

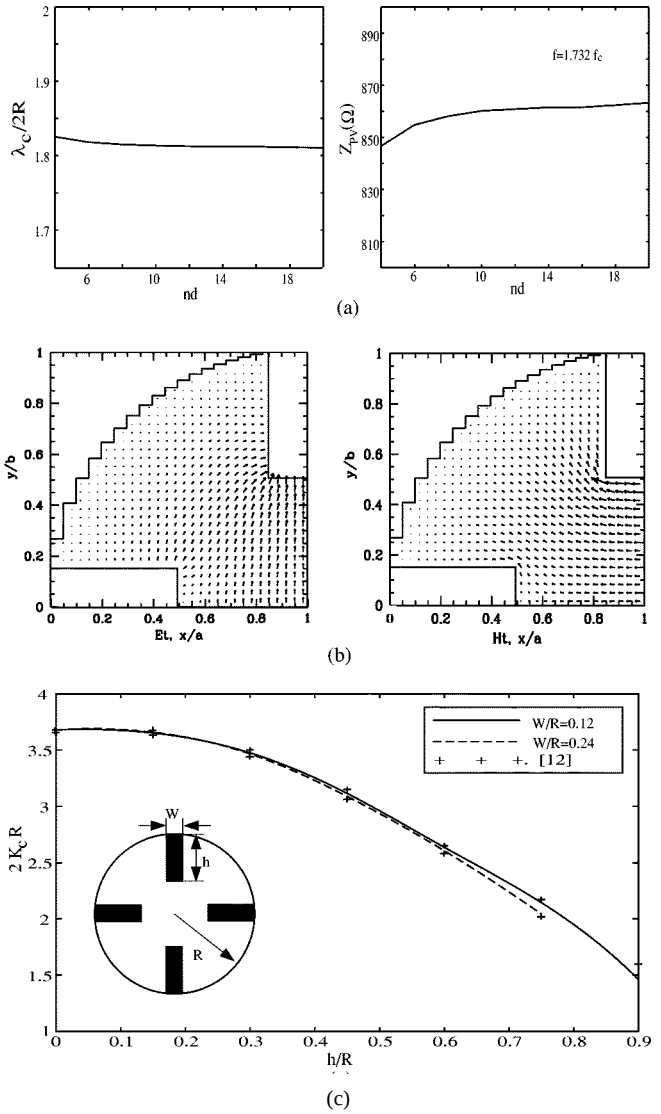

Fig. 11. (a) Convergence test of the cutoff wavelength and characteristic impedance Z_0 (v/p) of the dominant mode ($h/R = 0.3$, $w/R = 0.2$). (b) Electric- and magnetic-field distributions. (c) Comparison of the numerical results.

of the same cutoff frequency. However, the ridge–trough rectangular waveguide could have better attenuation and power-handling characteristics. The peaks in Fig. 8(b) result from the effect of the sidewall of the trough waveguide.

3) Cross-Finger Double-Ridge Rectangular Waveguides: As can be seen from Fig. 4, single-ridge rectangular waveguides have lower attenuation than double-ridge rectangular waveguides. However, the bandwidth and power handling are both poorer for the single-ridge rectangular waveguide than those in the double-ridge rectangular waveguides. In order to make full use of this property and the characteristics of the above discussed antipodal ridge rectangular waveguides, two new configurations of ridge waveguides are proposed whose characteristic are shown in Fig. 9. The new configuration has characteristics between those of antipodal ridge rectangular waveguides and those of double-ridge rectangular waveguides. The attenuation, dominant-mode cutoff wavelength, and power-handling capability could be all better than those

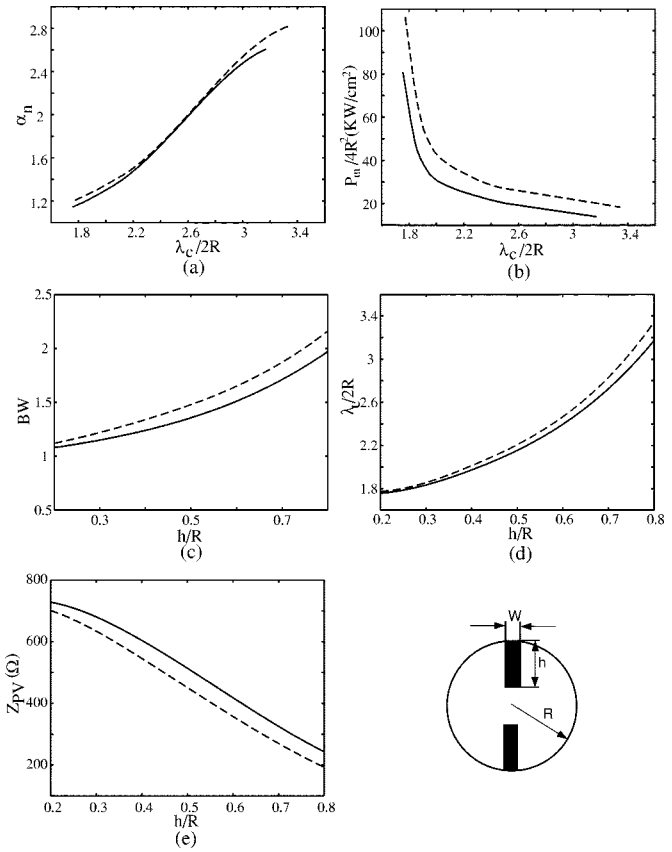

Fig. 12. (a) Attenuation, (b) power handling, (c) bandwidth, and (d) dominant-mode cutoff λ_C versus h/R. (e) Characteristic impedance at $f = \infty$ ($w/R = 0.1$, solid line; $w/R = 0.2$: dashed line).

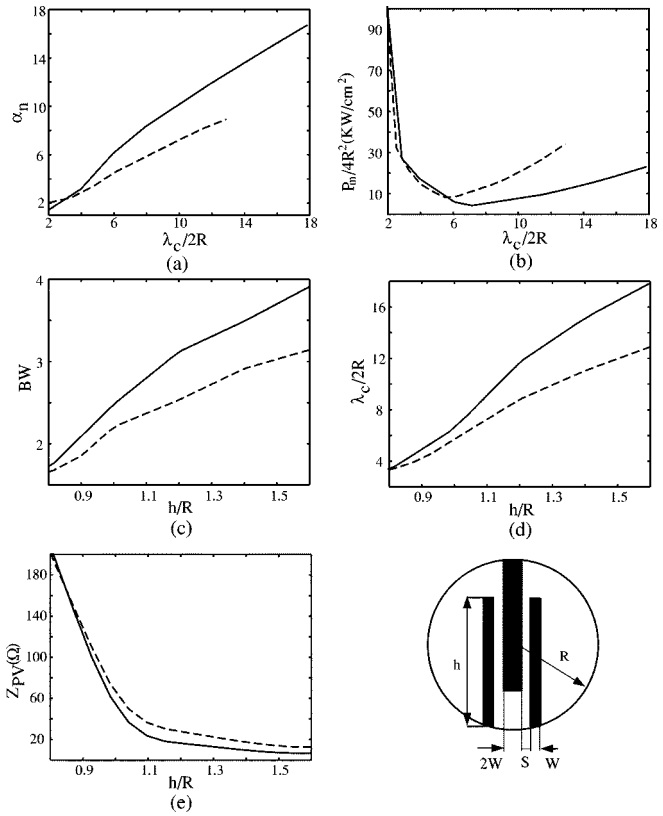

Fig. 13. (a) Attenuation, (b) power handling, (c) bandwidth, and (d) dominant-mode cutoff λ_C versus h/R. (e) Characteristic impedance at $f = \infty$ ($w/R = 0.1$: $s/R = 0.05$, solid line; $s/R = 0.1$: dashed line).

in single-ridge rectangular waveguides. Meanwhile, good bandwidth could be maintained. These two new configurations of ridge waveguides can be used in applications, where their superior characteristics justify their somewhat complex mechanical configurations.

4) Quadruple-Ridge Rectangular Waveguides: Quadruple-ridge waveguides find wide applications, especially in antenna and radar systems [9] because of their supporting dual-polarization capabilities. The attenuation and power-handling characteristics of the quadruple-ridge rectangular waveguides are shown in Fig. 10. Compared to the single-ridge rectangular waveguides, the attenuation becomes worse and the power handling improves. However, for the bandwidth, even compared to the regular rectangular waveguides, the bandwidth of quadruple-ridge waveguides is worse.

B. Circular-Ridge Waveguide

The above theory can also be applied to circular ridge waveguides. The boundary of the circular waveguide is approximated by a number of rectangular stairs. A quadruple-ridge circular waveguide, shown in Fig. 11, is presented as an example. Based on the symmetries of the waveguide cross section, only a quarter of the cross section needs to be analyzed. To check the accuracy of the numerical results, convergence is checked by increasing the number of divisions nd along the ridge. The division number along the other section is taken according to the ratio of h to $R - h$. Fig. 11(a) shows that the cutoff wavelength λ_c and the characteristic impedance Z_0 (v/p) converge as long as nd is taken larger than ten. Fig. 11(b) shows the dominant-mode field distributions in the waveguide. We can find that boundary conditions are all satisfied. Fig. 11(c) shows the comparison of the numerical results with published data [12]. Excellent agreement is achieved.

1) Double-Ridge and Double Antipodal Ridge Circular Waveguides: Figs. 12 and 13 show the attenuation and power-handling capabilities in the double-ridge and double antipodal ridge circular waveguides, respectively. Compared to the rectangular counterparts, both waveguides have better attenuation and power-handling characteristics. They can also provide large cutoff wavelength of the dominant-mode characteristics. However, double-ridge circular waveguides have little poor bandwidth characteristics because of the mode splitting. Also, double antipodal ridge waveguides could still have good bandwidth characteristics.

2) Quadruple-Ridge Circular Waveguides: Quadruple-ridge circular waveguides are also a type of widely used waveguides [13]. The characteristics of quadruple-ridge circular waveguides are presented in Fig. 14. It is interesting to find that, compared to their rectangular counterparts, the quadruple-ridge circular waveguides have better attenuation and power-handling capabilities. Compared to the regular circular waveguide, the bandwidth of quadruple-ridge circular waveguides can be improved by choosing the appropriate ridge widths and depths.

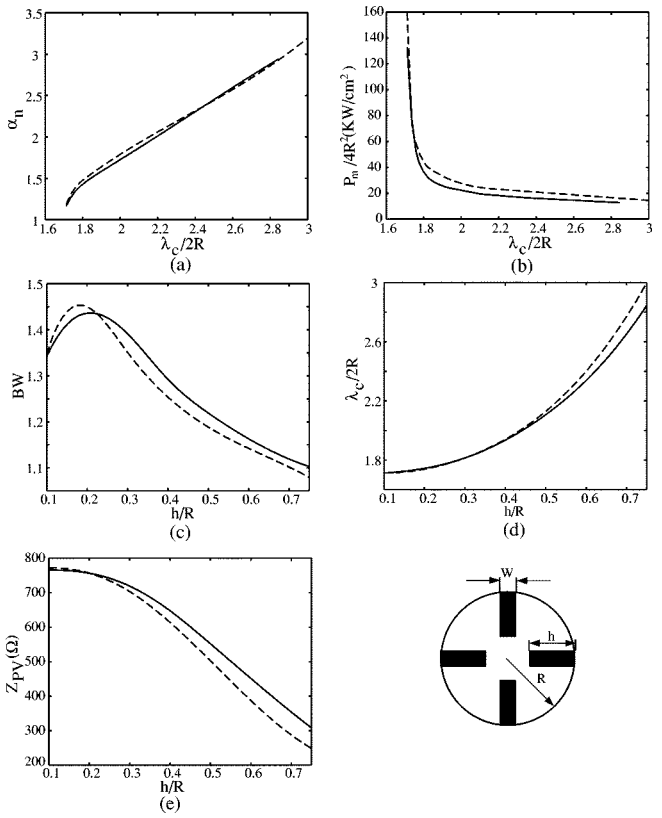

Fig. 14. (a) Attenuation, (b) power-handling, (c) bandwidth, and (d) dominant-mode cutoff λ_C versus h/R. (e) Characteristic impedance at $f = \infty$ ($w/R = 0.1$, solid line; $w/R = 0.2$: dashed line).

IV. Conclusion

The attenuation and power-handling in several ridge rectangular waveguides and ridge circular waveguides have been investigated in this paper, and numerical results for the characteristics of these waveguides were presented.

Numerical results have shown that for the ridge rectangular waveguides, attenuation and power handling in the antipodal ridge waveguides and the ridge–trough waveguides can be improved and dominant-mode cutoff wavelengths can be increased. Newly proposed cross-finger ridge waveguides have the characteristics between the double-ridge waveguide and the antipodal ridge waveguide. Compared to the single-ridge waveguides, cross-finger ridge waveguide could have better attenuation, power-handling, and longer dominant-mode wavelength characteristics and still maintain good bandwidth characteristics. The quadruple-ridge waveguides have worse attenuation and better power-handling capability properties. However, the bandwidth shrinks greatly.

For the circular-ridge waveguides, compared to the rectangular counterparts, double-ridge waveguides, double antipodal ridge waveguides, and quadruple-ridge waveguides all have better attenuation and power-handling capability characteristics. Double-ridge circular waveguides have somewhat poor bandwidth characteristics because of mode splitting. Double antipodal ridge waveguides and quadruple-ridge waveguide could have good bandwidth characteristics.

References

[1] S. B. Cohn, "Properties of ridge waveguide," *Proc. IRE*, vol. 35, no. 8, pp. 783–788, Aug. 1947.
[2] S. Hopfer, "The design of ridged waveguides," *IRE Trans. Microwave Theory Tech.*, vol. MTT-3, no. 10, pp. 20–29, Oct. 1955.
[3] P. K. Saha and G. G. Mazumder, "Bandwidth characteristics of inhomogeneous T-septum waveguides," *IEEE Trans. Microwave Theory Tech.*, vol. 37, pp. 1021–1026, June 1989.
[4] Y. Zhang and W. T. Joines, "Attenuation And power-handling capability of T-septum waveguides," *IEEE Trans. Microwave Theory Tech.*, vol. MTT-35, pp. 858–861, Sept. 1987.
[5] D. Dasgupta and P. K. Saha, "Rectangular waveguide with two double ridges," *IEEE Trans. Microwave Theory Tech.*, vol. MTT-31, pp. 938–941, Nov. 1983.
[6] ——, "Eigenvalue spectrum of rectangular waveguide with two symmetrically placed double ridges," *IEEE Trans. Microwave Theory Tech.*, vol. MTT-29, pp. 47–51, Jan. 1981.
[7] A. M. K. Saad, J. D. Miller, A. Mitha, and R. Brown, "Analysis of antipodal ridge waveguide structure and application on extremely wide stopband low-pass filter," in *IEEE MTT-S Int. Microwave Symp. Dig.*, 1986, pp. 361–363.
[8] A. M. K. Saad, "A unified ridge structure for evanescent-mode wide band harmonic filters: Analysis and applications," in *17th EUMC Proc.*, Rome, Italy, 1987, pp. 157–162.
[9] G. N. Tsandoulas and G. H. Knittel, "The analysis and design of dual-polarization square-waveguide phased arrays," *IEEE Trans. Antennas Propagat.*, vol. AP-21, pp. 796–808, Nov. 1973.
[10] W. Sun and C. A. Balanis, "MFIE analysis and design of ridged waveguides," *IEEE Trans. Microwave Theory Tech.*, vol. 41, pp. 1965–1971, Nov. 1993.
[11] M. H. Chen, G. N. Tsandoulas, and F. G. Willwerth, "Modal characteristics of quadruple-ridged circular and square waveguides," *IEEE Trans. Microwave Theory Tech.*, vol. MTT-22, pp. 801–804, Aug. 1974.
[12] W. Sun and C. A. Balanis, "Analysis and design of quadruple-ridged waveguides," *IEEE Trans. Microwave Theory Tech.*, vol. 42, pp. 2201–2207, Dec. 1994.
[13] C. C. Chen, "Quadruple ridge-loaded circular waveguide phased arrays," *IEEE Trans. Antennas Propagat.*, vol. AP-22, pp. 481–483, May 1974.
[14] U. Balaji and R. Vahldieck, "Radial mode matching analysis of ridged circular waveguides," *IEEE Trans. Microwave Theory Tech.*, vol. 44, pp. 1183–1186, July 1996.
[15] R. E. Collin, *Field Theory of Guided Waves*, 2 ed. New York: IEEE Press, 1991.
[16] H. W. Yao, K. A. Zaki, A. E. Atia, and R. Hershtig, "Full wave modeling of conducting posts in rectangular waveguides and its applications to slot coupled combline filters," *IEEE Trans. Microwave Theory Tech.*, vol. 43, pp. 2824–2830, Dec. 1995.
[17] R. Levy, "Power handling at microwave frequencies", to be published.
[18] C. W. Jones, "On the pulse length dependence of breakdown," MIT Lincoln Lab., Cambridge, MA, Tech. Rep. 46L-0027, May 23, 1962.
[19] N. Marcuvitz, *Waveguide Handbook*. Stevenage, U.K.: Peregrinus, 1986.
[20] D. Guha and P. K. Saha, "Some characteristics of ridge–trough waveguide," *IEEE Trans. Microwave Theory Tech.*, vol. 45, pp. 449–453, Mar. 1997.

Yu Rong (S'97–SM'99) was born in Jiangsu, China, in 1966. He received the B.S. and M.S. degrees both in radio engineering from Southeast University, Nanjing, China, in 1987 and 1990, respectively, and the Ph.D. degree in electrical and computer engineering from the University of Maryland at College Park, in 1999.

From 1990 to 1995, he was an Assistant Researcher/Lecturer in the Millimeter Wave Research Institute, Department of Electrical Engineering, Nanjing University of Science and Technology, Nanjing, China, where his research dealt mainly with the development of various microwave and millimeter-wave components and systems. From 1995 to 1999, he was a Research Assistant under the direct guidance of Dr. K. A. Zaki in the Microwave Laboratory, Department of Electrical and Computer Engineering, University of Maryland at College Park. His current research interests include analysis and design of various microwave and millimeter-wave components and subsystems (front-ends). He is currently with Paratek Microwave Inc., Columbia, MD, where he is involved with the development of RF, microwave and millimeter-wave tunable filters, and millimeter-wave phased-array antennas.

Kawthar A. Zaki (SM'85–F'91) received the B.S. degree (with honors) from Ain Shams University, Cairo, Egypt, in 1962, and the M.S. and the Ph.D. degrees from the University of California at Berkeley, in 1966 and 1969, respectively, all in electrical engineering.

From 1962 to 1964, she was a Lecturer in the Department of Electrical Engineering, Ain Shams University. From 1965 to 1969, she was a Research Assistant in the Electronics Research Laboratory, University of California at Berkeley. In 1970, she joined the Electrical Engineering Department (now the Electrical and Computer Engineering Department), University of Maryland at College Park, where she is currently a Professor of electrical engineering. Her research interests are in the areas of electromagnetics, microwave circuits, simulation, optimization, and computer-aided design of advanced microwave and millimeter-wave systems and devices. She has authored or co-authored over 200 publications in her areas of research interests, and holds five patents on filters and dielectric resonators.

Dr. Zaki has received several academic honors and awards for teaching, research, and inventions.